International Journal of Infrared and Millimeter Waves, Vol. 21, No. 9, 2000

IMPROVED COMPUTER PROGRAM FOR MAGNETRON INJECTION GUN DESIGN

Yi Sheng Yeh,[1] Ming Hsiung Tsao,[2] Han Ying Chen,[3] and Tsun-Hsu Chang[2]

[1]*Department of Electrical Engineering*
Southern Taiwan University of Technology
Tainan, Taiwan
[2]*Department of Physics*
National Tsing Hua University
Hsinchu, Taiwan
[3]*Electronics Research and Service Organization*
Industrial Technology Research Institute
Hsinchu, Taiwan

Received May 21, 2000

ABSTRACT

Gyrotron has received extensive attention owing to its high-power capability, especially when the wavelength shrinks below the millimeter-wave range. The electron beam of a gyrotron is typically generated by a magnetron injection gun (MIG). For high cathode current density, the MIG may operate in a region that combines temperature limited and space-charge limited emissions. An improved computer program for electron gun design is appropriate for MIGs that operate between space-charge limited and temperature limited emission. Moreover, the initial input formation of the program resembles that of the EGUN code. Analysis of a Pierce electron gun and MIGs reveals that the simulated beam current appears consistent with the measured results. However, EGUN simulation results in which the cathode emitters of MIGs are chosen for the temperature limited emission differ from those of our simulation results. This difference is most likely owing to that the initial emitting energy can not be completely described in the EGUN simulation. Finally, the improved computer program is used to design a MIG for a Ka-band, TE_{01} mode gyro-TWT.

Key words: magnetron injection gun, space-charge limited emission, temperature limited emission, gyrotron, gyro-TWT

0195-9271/00/0900-1397$18.00/0

I. INTRODUCTION

A variety of gyrodevices based on fast-wave interaction structure, such as gyrotrons, the peniotrons, and the cyclotron autoresonance maser, are subjects of current interest because of their capability for high-power millimeter-wave generation [1]. The electron beam for such devices is typically generated by a magnetron injection gun. In a MIG (Fig. 1), electrons originate from a ring-shaped thermionic emitter mounted on the cathode. An electric field extends between the cathode and the anode and a static magnetic field is applied to bend, as well as focus the electrons. As soon as the electrons leave the cathode, they experience a crossed electric and magnetic field, and therein obtain the spiral motion. The electrons, thus, form an annual beam with electrons executing small cyclotron orbits as required for the cyclotron resonance interaction.

In many gyro-TWTs, the operating points of the MIGs are chosen to be located in the temperature limited region [1]-[5]. The development of a high frequency and high power gyrotron is current of time, so the cathode current density of the gyrotron is increased. The potential in front of the emitting surface is decreased owing to the space-charge effect. The cathode current is not dominated by the cathode temperature. Thus, the space-charge effects in front of the emitting surface are important to a MIG design.

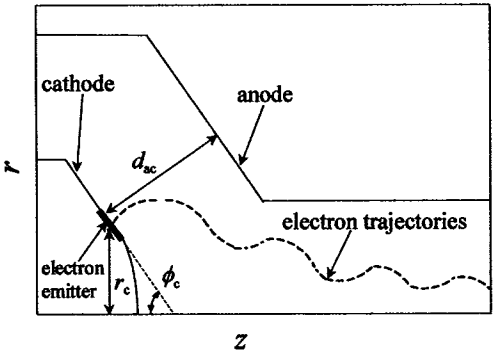

Fig. 1. Schematic of a MIG.

Baird and Lawson [2] suggested that the operating point of the MIG is estimated by the ratio of the temperature limited cathode current density J_{TL} to the Langmuir space-charge limited current density J_{SC} in the trade-off equations. The design with $J_{TL}/J_{SC} < 15\%$ is typically free of space-charge problems [6], but the value of J_{TL}/J_{SC} obtained using this method is only an estimate. The value is not accurate owing to the conical electrode approximation, a narrow strip cathode, and neglecting magnetic field in utilized in the gun.

Longo [7] found that the operating point of the thermionic emitter is usually the transition from the temperature limited to space-charge limited region. An empirical law has been employed by Longo to study the cathode current density as a combination of both temperature limited and space-charge limited current density.

To accurately determine beam quality, a computer program is essential for electron gun design. Although the SCLA electron trajectory program EGUN [8] is extensively used to simulate the electron trajectories of a gun, the operating point of the gun is restricted to the temperature limited or space-charge limited region. A variable mesh finite element program [9], [10] has been developed to simulate the trajectories of the electron beam. Although the computer program is appropriate for operating between the temperature limited and space-charge limited emission, mesh generation is the most tedious and time-consuming aspect of the program. Therefore, the main goal is to develop a computer program which overcomes the above disadvantages.

This paper presents an improved computer program for electron gun design to simulate electron trajectories. The program permits operating regions between temperature limited and space-charge limited emission, and the initial input formation of the program is described using the input formation of EGUN code. The simulated space-charge current density calculated by the program replaces the Langmuir space-charge current density, allowing the operating region of the cathode emitter to be

estimated correctly.

The rest of this paper is organized as follows. Section II describes the computer model of the program. Section III presents the beam characteristics of a Pierce electron gun and MIGs. The measured results of the beam current obtained from the laboratory electron gun are presented and compared with the simulation predictions. Moreover, our simulation results are compared with the EGUN simulation results. Next, Section IV employs the improved computer program to design a MIG for a Ka-band, TE_{01} mode gyro-TWT. The beam power of the MIG approach 1.8 MW. The beam characteristic of the optimized MIG design is also presented. Conclusions are finally made in Section V.

II. COMPUTER MODEL

The computer program is specifically designed to calculate electron trajectories in electrostatic and magnetostatic fields. In the steady state, the potential according to the Poisson equation can be expressed as

$$\nabla^2\Phi = -\frac{\rho}{\varepsilon_0}, \tag{1}$$

where Φ is the electrostatic potential, ρ is the space-charge density, and ε_0 is the permittivity in the vacuum. The Poisson equation is solved by the finite different method. Meanwhile, the semi-iterative Chebyshev method is used to reduce the calculation time [8].

The electron trajectories are determined by the relativistic force equation using the fourth-order Runge-Kutta method [8]

$$m\frac{d}{dt}(\gamma\mathbf{v}) = e\nabla\Phi - e\mathbf{v}\times\mathbf{B}, \tag{2}$$

where m is electron mass, γ is a factor of relativity, $\mathbf{v}$ is the velocity of electron, e is the magnitude of electron charge, and $\mathbf{B}$ is the total magnetic field including external and self-consisting magnetic fields.

The operating point of the cathode emitter may be the region

between the temperature limited and space-charge limited emission, so the cathode current density J_c from Longo's empirical formula can be expressed as a combination of the temperature limited current density J_{TL} and space-charge limited current density J_{SC} [10]

$$J_c = \frac{J_{SC} + J_{TL}}{J_{SC} J_{TL}}. \tag{3}$$

The J_{SC} and J_{TL} calculated from Langmuir's and Richardson's laws [10] are written as

$$J_{SC} = k\frac{\Phi^{3/2}}{d^2}, \tag{4}$$

$$J_{TL} = 1.2\times10^4 T^2 \exp(\frac{-11600W}{T})\exp(0.44\frac{\sqrt{E_n}}{T}), \tag{5}$$

where $k = (4/9)\varepsilon_0\sqrt{(2e/m)} = 2.335\times10^{-6}$ (MKS), d is the normal distance from cathode (cm), W is the cathode work function (eV), T is the temperature of cathode ($^{\circ}$K), and E_n is the component of the electric field normal to the cathode (V/m).

When the electric field is not large enough near the cathode, the space-charge effects which build up in front of the cathode depress the potential in front of the emitting surface. If the electric field is zero in front of the emitting surface, the virtual cathode is established [9]. To simplify calculation, the proposed simulation assumes that the separation between the simulated and cathode emitting surface is about 1~2 mesh units. The initial velocity of the electron on the simulated emitting surface can be written as [8]

$$v_i = c\sqrt{\frac{\Phi(\Phi+2\lambda)}{(\Phi+\lambda)^2}}, \tag{6}$$

$$\theta_i = \cos^{-1}\left(\frac{E_z}{E}\right), \tag{7}$$

where $\lambda = mc^2/e$, and c is the velocity of light, θ_i is the angle between the initial velocity and the longitudinal axis, E_z is the longitudinal

magnitude of the electric field, and E is the magnitude of the electric field.

The space charge density ρ can be written as [8]

$$\rho = \frac{J}{v}, \tag{8}$$

where J is the current density, and v is the magnitude of the electron velocity.

It was determined empirically by True [9] that a numerically unstable oscillation can be established by slowly varying variables, such as potential, and cathode current density, which do not change enough to affect the rapidly changing variables, such as space charge. To suppress this numerical instability, the cathode current density of the emitting surface is written as [9]

$$\bar{J}_m = \frac{1}{4}(J_{m^-} + 2J_m + J_{m^+}), \tag{9}$$

$$\bar{J}_m^{(\text{new})} = \bar{J}_m^{(\text{old})} + \omega(\bar{J}_m - \bar{J}_m^{(\text{old})}), \tag{10}$$

where ω is a computer parameter, J_{m^-}, J_m, and J_{m^+} are the cathode current densities of the different points on the simulated emitting surface (Fig. 2), and $\bar{J}^{(\text{old})}$, $\bar{J}^{(\text{new})}$ are the cathode current densities on the simulated emitting surface from the pervious and latter iterations,

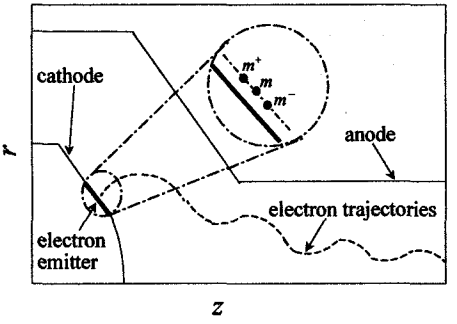

Fig. 2. Schematic of the relative locations of the points m^-, m, and m^+ on the simulated emitting surface.

respectively. If $\overline{J}_m$ is negative, arising from negative potential in front of the emitting surface, an alter scheme is employed [9]

$$\overline{j}_m^{(\text{new})} = \xi\, \overline{j}_m^{(\text{old})}, \tag{11}$$

$$\Phi^{(\text{new})} = \xi\, \Phi^{(\text{old})}, \tag{12}$$

$$\mathbf{E}^{(new)} = \xi\, \mathbf{E}^{(old)}, \tag{13}$$

where ξ is also a computer parameter to depress the numerical instability.

The computer program for electron gun design is developed from the above computer models . The final output parameters of the program include beam current, cathode current density, electron trajectories, average velocity, velocity spread, average guiding center radius, and average Larmor radius.

III. NUMERICAL SIMULATION AND EXPERIMENTAL VERFICATION

A. A Pierce electron gun

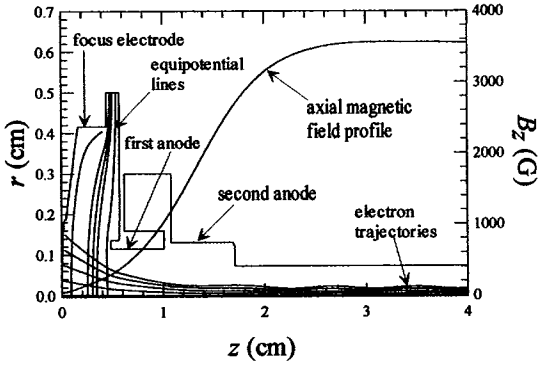

Fig. 3. Schematic of a Pierce electron gun and calculated electron trajectories. Also shown are the equipotential lines and the magnetic field profile. Radial and horizontal axes are scaled in unit of 0.01 cm.

A Pierce electron gun [11] was developed by NTHU for an Ku-band extended interaction oscillator (EIO). The operating parameters of the EIO were V_b=16.02 kV, I_b=0.49 A, and P(peak output power)=1.41 kW at 18.0% electric efficiency.

Figure 3 shows a computer drawn cross-section of the final Pierce electron gun configuration along with electron trajectories and a superimposed plot of the axial magnetic field profile. The required beam current approaches the space-charge limited current of the gun. Therefore, the cathode temperature does not dominate the beam current. The measured perveance of the gun is about 0.24 μp [11]. Our simulation result corresponds to the experimental and EGUN simulation results. Therefore, the improved computer program appears to be appropriate for Pierce electron guns design.

B. Magnetron injection guns

A magnetron injection gun [12] was developed by NTHU for an Ka-band, TE_{11} mode gyro-TWT. The specifications of the gyro-TWT were

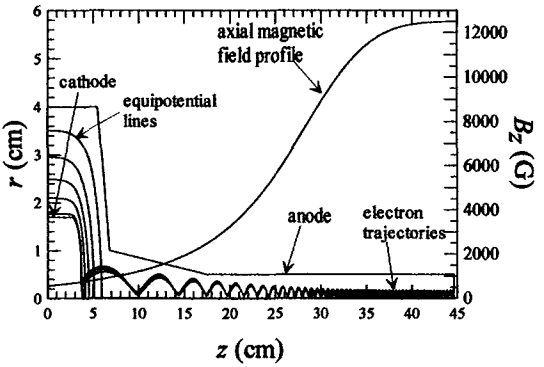

Fig. 4 Schematic of a MIG for a Ka-band, TE_{11} mode gyro-TWT and calculated electron trajectories. Also shown are the equipotential lines and the magnetic field profile. Radial and horizontal axes are scaled in unit of 0.025 cm.

V_b=95 kV, I_b=2 A, B_0=12.5 kG, α=0.9, and $\Delta v_z / v_z < 4\%$. Figure 4 shows a computer drawn cross-section of the final MIG configuration along with electron trajectories and a superimposed plot of the axial magnetic field profile. Table I lists the EGUN simulation results and our simulation results. The average velocity ratio α and axial velocity spread $\Delta v_z / v_z$ are larger for our simulation than that for the EGUN simulation.

In EGUN and our simulation, the separation between the simulated and cathode emitter is about 1~2 mesh units for numerical calculation. In our simulation, the initial energy of electrons on the simulated emitting surface are obtained by their potential. Figure 5a also shows that the initial energy of electrons on the simulated emitting surface is non-uniform and is not neglected in our simulation. EGUN simulation assumes the initial emitting electron energy to be uniform in the simulated emitting surface. If the initial energy of electrons on the simulated emitting surface is fixed at about 1150 eV in EGUN simulation, the results approach those of our simulation (Fig. 5b). This phenomenon indicates that the EGUN simulation is consistent with our simulation if the initial emitting electron energy is assumed to be prompt. Therefore, we believe that the discrepancy between EGUN simulation and our simulation can be attributed to the initial emitting electron energy not being completely described in EGUN simulation. To test this hypothesis, Figure 6 presents another case of a MIG for Ka-band, TE_{21} mode, second harmonic gyro-TWT. The specifications of the gyro-TWT are V_b=90 kV, I_b=20 A, and B_0=6.4 kG. Table II lists the EGUN simulation results and our simulation results. If the initial energy of electrons on the simulated emitting surface is chosen to be about 825eV, the EGUN results approach our simulation results (Fig. 7a and 7b). Tables I and II indicate that the discrepancy of beam quality between EGUN and our simulations is less for the MIG design (Fig. 6) than that for the above MIG design (Fig. 4). This phenomenon is most likely owing to that the difference of the initial emitting electron energy between EGUN and our simulations is less for

Table I. The beam characteristics of a MIG for a Ka-band, TE_{11} mode gyro-TWT.

parameter	EGUN simulation	Our simulation
Initial emitting electron energy	0.10 eV	1746 ~ 2208eV
Temperature limited current I_{TL}	2.00 A	2.06 A
Space-charge limited current I_{SC}	... [a]	66.6 A
Beam current I_b	2.00 A	2.00 A
Average axial velocity ratio $\langle v_z / c \rangle$	0.388	0.359
Average perpendicular velocity ratio $\langle v_\perp / c \rangle$	0.359	0.395
Average velocity ratio α	0.928	1.10
Average guiding center radius $\langle r_g \rangle$	0.935 mm	0.970 mm
Average Larmor radius $\langle r_L \rangle$	0.577 mm	0.636 mm
Axial velocity spread $\Delta v_z / v_z$	3.86 %	4.69 %
Perpendicular velocity spread $\Delta v_\perp / v_\perp$	5.14 %	4.14 %

[a] The emitter of the MIG is chosen to be temperature limited emission in EGUN simulation.

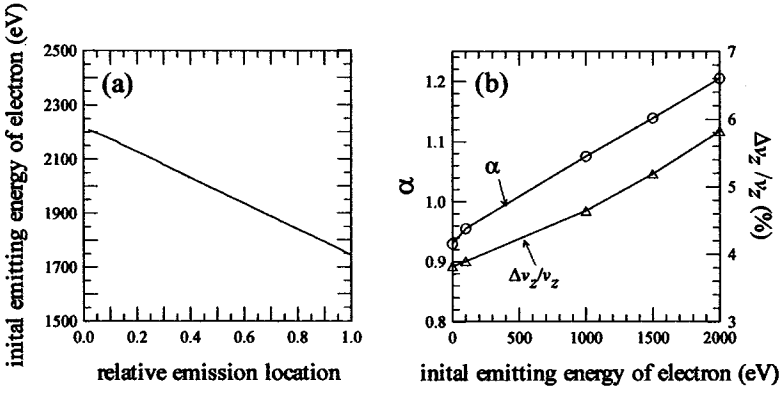

Fig. 5. (a) displays simulated initial emitting energy of electron as functions of the relative emission location of a MIG in our simulation. (b) displays simulated average velocity ratio α and axial velocity spread $\Delta v_z / v_z$ as functions of the initial emitting energy of electron of a MIG in EGUN simulation. The schematic of the MIG is shown in Fig. 4.

the MIG design than that for the above MIG design.

Figure 8 shows the simulated and measured beam currents of the above MIG design (Fig. 4). As Figure 8a presents, the space-charge limited current increases with the anode voltage. Meanwhile Figure 8b displays the measured results of the gun. The heater power P_h is applied to heat the cathode emitter. Thus the cathode temperature goes up with increasing heater power. The simulation results are consistent with the measured results. The improved program proves to be appropriate for simulating the beam characteristics as the transition between temperature limited and space-charge limited regimes.

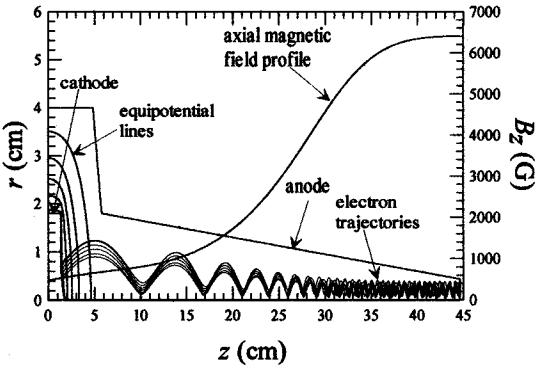

Fig. 6. Schematic of a MIG for a Ka-band, TE_{21} mode, second harmonic gyro-TWT and calculated electron trajectories. Also shown are the equipotential lines and the magnetic field profile. Radial and horizontal axes are scaled in unit of 0.025 cm.

Table II. The beam characteristics of a MIG for a Ka-band, TE_{21} mode, second harmonic gyro-TWT.

parameter	EGUN simulation	Our simulation
Initial emitting electron energy	0.1eV	794~1376 eV
Temperature limited current I_{TL}	20.5 A	24.1 A
Space-charge limited current I_{SC}	...[a]	142 A
Beam current I_b	20.5 A	20.5 A
Average axial velocity ratio $\langle v_z/c \rangle$	0.364	0.350
Average perpendicular velocity ratio $\langle v_\perp/c \rangle$	0.397	0.412
Average velocity ratio α	1.13	1.23
Average guiding center radius $\langle r_g \rangle$	2.12 mm	2.14 mm
Average Larmor radius $\langle r_L \rangle$	1.26 mm	1.31 mm
Axial velocity spread $\Delta v_z/v_z$	13.4 %	14.8 %
Perpendicular velocity spread $\Delta v_\perp/v_\perp$	11.5 %	10.7 %

[a] The emitter of the MIG is chosen to be temperature limited emission in EGUN simulation.

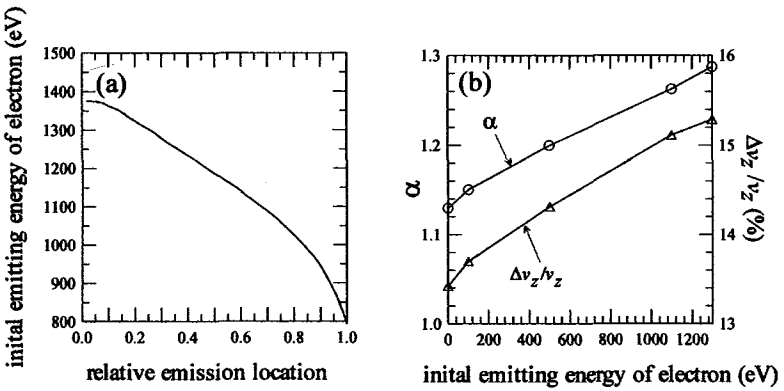

Fig. 7. (a) displays simulated initial emitting energy of electron as functions of the relative emission location of a MIG in our simulation. (b) displays simulated average velocity ratio α and axial velocity spread $\Delta v_z/v_z$ as functions of the initial emitting energy of electron of a MIG in EGUN simulation. The schematic of the MIG is shown in Fig. 6.

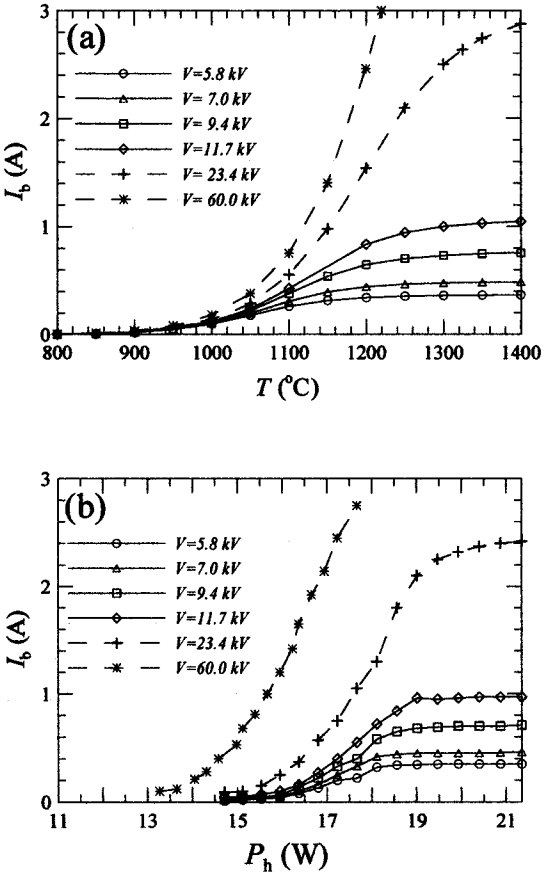

Fig. 8. (a) displays the simulated beam current at six values of anode voltage as functions of the cathode temperature. The work function of the cathode is fixed to be 2.025 eV. (b) displays the measured beam current at six values of anode voltage as functions of the heater power. The schematic of the MIG is shown in Fig. 4.

IV. A MAGNETRON INJECTION GUN FOR A KA-BAND, TE_{01} MODE GYRO-TWT

Figure 9 displays an optimized MIG design for a Ka-band, TE_{01} mode gyro-TWT. The specifications of gyro-TWT are V_b=90 kV, I_b=20 A, B_0=12.8 kG, α=0.9, $\Delta v_z / v_z$<5%, and r_g=0.28 cm [13]. Tables III and IV list the optimized design parameters and the beam characteristics, respectively. The ratio of I_{TL} / I_{SC} is 5.34%, meaning the operating point of the gun seems to approach temperature limited emission.

Figure 10a shows that the initial energy of the electron on the simulated emitting surface is about 1700~2656 eV. As Figure 10b shows, the cathode current density of the MIG is non-uniform. The simulation results of the beam characteristics should be influenced by the above phenomenon.

Figure 11 shows the variation of the beam quality with axial location in the MIG. An increase in the axial magnetic field caused the α value to increase. The velocity spreads are closely related to the axial magnetic field. Figure 12 presents the dependence of the velocity ratio α on the relative location of the emitter. The fluctuation of the velocity ratio α may be attributed to high cathode current density.

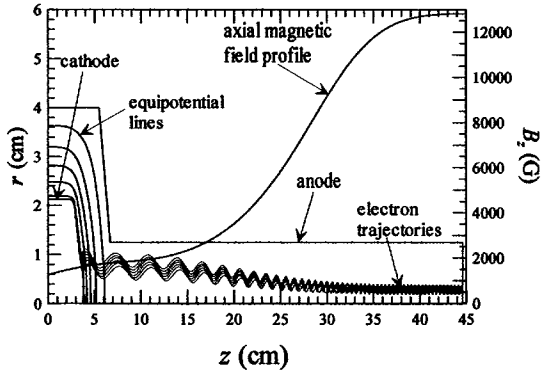

Fig. 9. Schematic of a MIG for a Ka-band, TE_{01} mode gyro-TW and calculated electron trajectories. Also shown are the equipotenti lines and the magnetic field profile. Radial and horizontal axes a scaled in unit of 0.025 cm.

Table III. The electrode specifications of a MIG for a Ka-band, TE_{01} mode gyro-TWT.

Cathode radius r_c	7.66 mm
Emitter strip width l_s	3.75 mm
Cathode-anode gap d_{ac}	30 mm
Cathode tilt angle ϕ_c	48.8°
Compression ratio f_m	8.00
Average cathode current density J_c	11.1 A/cm^2

Table IV. The beam characteristics of a MIG for a Ka-band, TE_{01} mode gyro-TWT.

Initial emitting electron energy	1700~2656 eV
Temperature limited current I_{TL}	21.1 A
Space-charge limited current I_{SC}	395 A
Beam current I_b	20.0 A
Average axial velocity ratio $\langle v_z/c \rangle$	0.385
Average perpendicular velocity ratio $\langle v_\perp/c \rangle$	0.344
Average velocity ratio α	0.897
Average guiding center radius $\langle r_g \rangle$	2.85 mm
Average Larmor radius $\langle r_L \rangle$	0.534mm
Axial velocity spread $\Delta v_z/v_z$	4.52 %
Perpendicular velocity spread $\Delta v_\perp/v_\perp$	5.53 %

V. CONCLUSIONS

This paper presents an improved computer program for simulating the beam characteristics of electron guns. Comparing the experimental and EGUN simulation results suggests that the cathode, which is the temperature limited emission, can not be

completely described in EGUN simulation. The phenomenon appears to become obvious when the potential in front of the emitting surface is sufficiently large. Finally, the improved computer program develops an optimal MIG design for a Ka-band, TE_{01} mode gyro-TWT.

We recommend conducting experiments for measuring the beam quality, such as velocity ratio α, and axial velocity spread $\Delta v_z / v_z$. The results might help clarify the effectiveness of the improved computer program.

ACKNOWLEDGMENTS

The authors would like to thank Prof. K.R. Chu, and Prof. C.C. Sah for their valuable assistance and cooperation. This work was supported by the National Science Council of the Republic of China (NSC-89-2213-E-218-006).

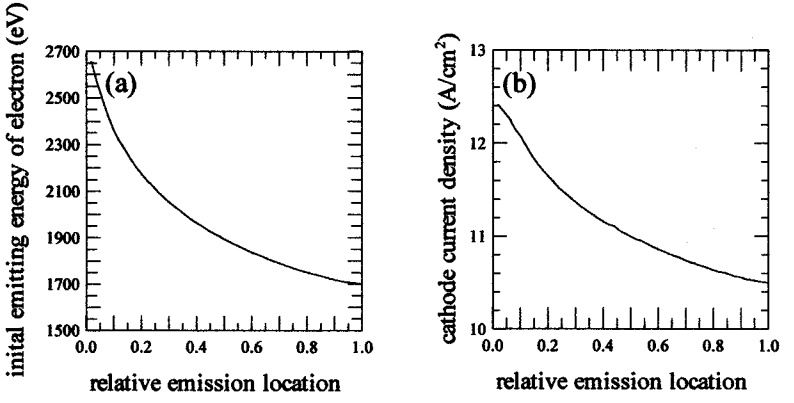

Fig. 10. (a) displays simulated initial emitting energy of electron as functions of the relative emission location of a MIG in our simulation. (b) displays simulated cathode current density as functions of the relative emission location of a MIG in our simulation. The schematic of the MIG is shown in Fig. 9.

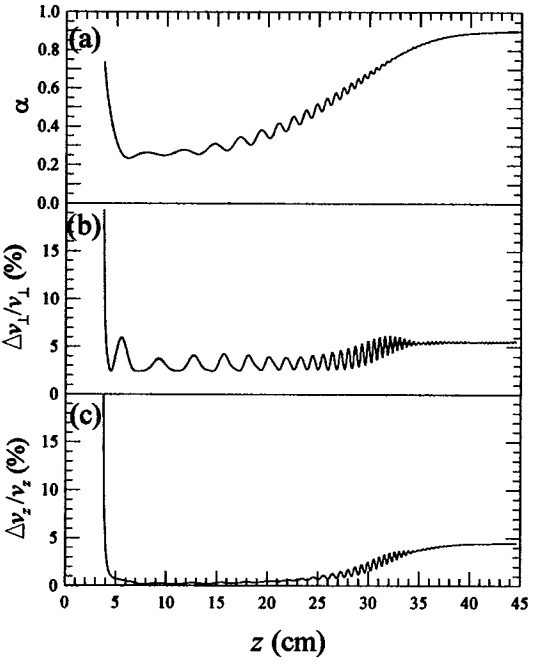

Fig. 11. (a), (b), and (c) display the simulated average velocity ratio α, perpendicular velocity spread $\Delta v_\perp / v_\perp$, and axial velocity spread $\Delta v_z / v_z$ of a MIG as functions of the axial location z in our simulation. The schematic of the MIG is shown in Fig.9.

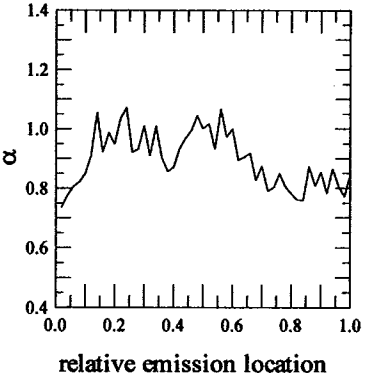

Fig. 12. Simulated average velocity ratio α as functions of the relative emission location of a MIG in our simulation. The schematic of the MIG is shown in Fig. 9.

REFERENCES

[1] J.L. Sefter, A.T. Drobot, and K.R. Chu, "An investigation of a magnetron injection gun suitable for use in cyclotron resonance maser," *IEEE Trans. Electron Devices*, vol. ED-26, no. 10, pp. 1609-1616, 1979.

[2] J.M. Baird and W. Lawson, "Magnetron injection gun (MIG) design for gyrotron applications," *Int. J. Electron.*, vol. 61, no. 6, pp. 953-967, 1986.

[3] K.R. Chu, L.R. Barnett, W.K. Lau, L.H. Chang, and H.Y. Chen, "A wide-band millimeter-wave gyrotron traveling wave amplifer experiment," *IEEE Trans. Electron Devices*, vol. 37, no. 6, pp. 1557-1560, 1990.

[4] Ch Wang, Y.S. Yeh, T.T. Yang, H.Y. Chen, S.H. Chen, Y.C. Tsai, L.R. Barnett, and K.R. Chu, "A mechanically tunable magnetron injection gun," *Rev. Sci. Instruments*, vol. 68, no. 8, pp. 3031-3035 ,1997.

[5] K.R. Chu, H.Y. Chen, C.L. Hung, T.H. Chang, L.R. Barnett, S.H. Chen, and T.T. Yang, "Ultrahigh gain gyrotron traveling wave amplifer," *Phys. Rev. Lett.*, vol. 81, no. 21, pp. 4760-4763, 1998.

[6] W. Lawson, J. Calame, V.L. Granatstein, G.S. Park, C.D. Striffler, and J. Neilson, "The design of a high peak power relativistic magnetron injection gun," *Int. J. Electron.*, vol. 61, no. 6, pp. 969-984, 1986.

[7] R.T. Longo, "A study of thermionic emitters in the regime of partical operation," *Int. Electron Devices Mtg.*, p467-470, 1980.

[8] W.B. Herrmannsfeldt, *Electron Trajectory Program*, Standford Linear Accelerator Center Report SLAC-226, 1979.

[9] R.B. True, *Space-charge-limited beam forming systems analysed by the method of self-consistent fields with solution of Poisson's equation on a deformable relation mesh*, Ph.D. thesies, University of

Connecticut, 1972.

[10] M. Caplan and C. Thorington, "Improved computer modelling of magnetron injection guns for gyrotrons," *Int. J. Electron.*, vol. 51, no. 4, pp. 415-426, 1981.

[11] L. Chen, H. Guo, H.Y. Chen, M.H. Tsao, T.T. Yang, Y.C. Tsai, and K.R. Chu, "An extended interaction oscillator based on a complex resonator structure," accepted for publication in the 8th special issue on high power microwaves in the *IEEE Trans Plasma Science*, 9 Mar 2000.

[12] L.R. Barnett, L.H. Chang, H.Y. Chen, K.R. Chu, W.K. Lan, and C.C. Tu, "Absolute instability competition and suppression in a millimeter-wave gyrotron traveling-wave tube," *Phys. Rev. Lett.*, vol. 63, no. 10, pp. 1062-1065, 1989.

[13] T.H. Chang, *The operating point of Ka-band gyro-TWT*, NTHU RF Lab. Report, 1999.